

Unconventional bulk superconductivity in YFe_2Ge_2 single crystals

Jiasheng Chen,¹ Monika B. Gamza,² Jacintha Banda,³ Keiron Murphy,^{1,*} James Tarrant,¹ Manuel Brando,³ and F. Malte Grosche¹

¹*Cavendish Laboratory, University of Cambridge, Cambridge CB3 0HE, United Kingdom*

²*Jeremiah Horrocks Institute for Mathematics, Physics and Astronomy, University of Central Lancashire, Preston, United Kingdom*

³*Max Planck Institute for Chemical Physics of Solids, Nöthnitzer Straße 40, 01187 Dresden, Germany*

(Dated: November 10, 2021)

Using a new horizontal flux growth technique to produce high quality crystals of the unconventional superconductor YFe_2Ge_2 has led to a seven-fold reduction in disorder scattering, resulting in mm-sized crystals with residual resistivities $\simeq 0.45 \mu\Omega \text{ cm}$, resistivity ratios $\simeq 430$ and sharp superconducting heat capacity anomalies. This enables searching multi-probe experiments investigating the normal and superconducting states of YFe_2Ge_2 . Low temperature heat capacity measurements suggest a significant residual Sommerfeld coefficient, consistent with in-gap states induced by residual disorder as predicted for a sign-changing order parameter.

The iron-based layered compound YFe_2Ge_2 has been reported as a new unconventional superconductor [1], which differs from other iron-based superconductors by its lack of group-V (pnictogen) or group-VI (chalcogen) elements and its more three dimensional Fermi surface geometry [2, 3]. Nevertheless, YFe_2Ge_2 shares key properties of the alkali metal iron arsenides, $(\text{K}/\text{Cs}/\text{Rb})\text{Fe}_2\text{As}_2$: (i) similarly enhanced Sommerfeld coefficient, $C/T \sim 100 \text{ mJ/mol K}^2$ [4–6]; (ii) bad metal behavior at room temperature, with resistivity ρ of order $200 \mu\Omega \text{ cm}$ [7]; (iii) strong suppression of the superconducting transition temperature T_c by disorder scattering [8]. The highly correlated low temperature state and its crossover to incoherent bad metal behavior at high temperature [9–11] have been attributed to Hund's coupling, which forces the iron d-electrons into a high spin state, causing strong correlations and leading to narrow bands independently of the shape of the Fermi surface [12]. Initially, no heat capacity anomalies were observed at the superconducting transition in polycrystals [13] or single crystals [14], despite considerable efforts on optimizing the crystal growth. Further, systematic improvements of polycrystal quality produced the first thermodynamic evidence of bulk superconductivity in YFe_2Ge_2 [15], clarified the primary origin of crystalline imperfections in YFe_2Ge_2 and demonstrated that disorder rapidly suppresses the transition at a rate commensurate with expectations for a sign-changing order parameter [16]. This motivated a renewed effort to produce bulk superconducting single crystals that are required for specialised experiments probing the strongly correlated normal state and the superconducting gap symmetry in YFe_2Ge_2 .

Here, we describe modified flux growth techniques which produce YFe_2Ge_2 single crystals of superior quality, with residual resistivity $\rho_0 < 0.45 \mu\Omega \text{ cm}$ and residual resistance ratio $\text{RRR} \equiv \rho(300 \text{ K})/\rho_0 \sim 430$, establishing horizontal liquid transport as a powerful method for producing ultra-high quality crystals of challenging materials. Our crystals, for the first time, display sharp signa-

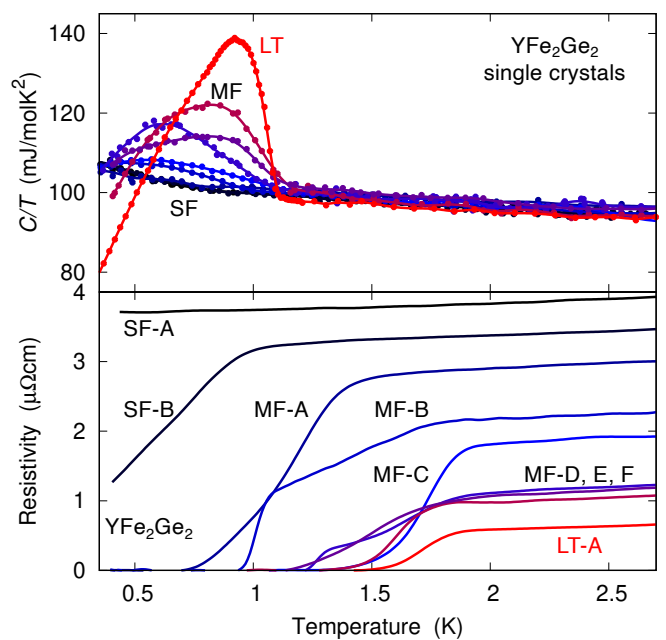


Figure 1. Sommerfeld ratio of the heat capacity C/T (upper panel) and electrical resistivity (lower panel) of YFe_2Ge_2 single crystals from different growth batches. SF=standard flux growth, MF=modified flux growth, LT=liquid transport growth. These samples show a wide variation in their heat capacity superconducting anomaly, resistive transition and residual resistivity. Lower residual resistivities correlate with sharper superconducting heat capacity anomalies.

tures of the superconducting transition in heat capacity, magnetisation and resistivity, proving that superconductivity is indeed intrinsic to YFe_2Ge_2 of sufficient quality. We find that the size of the superconducting heat capacity anomaly and the extrapolated residual Sommerfeld ratio $\gamma_0 = \lim_{T \rightarrow 0} C/T$ correlate strongly with the disorder level and that γ_0 displays a further, distinct dependence on applied magnetic field. These results are consistent with unconventional superconductivity with a

sign-changing gap function.

Methods – Our crystal growth experiments are designed to enhance Fe occupancy on the Fe site, which in polycrystals proved to be the determining factor for achieving low disorder [16]. A comprehensive crystal growth study using the conventional Sn-flux method demonstrated that lowering the growth temperatures leads to higher quality [14, 17]. This has motivated our approach, which reduces the temperature at which crystals precipitate from the melt by increasing the effective flux to charge ratio. Multiple batches of YFe_2Ge_2 single crystals have been grown with Sn-flux methods using (i) standard flux growth (SF) as described in [18] and used in previous crystal growth studies on YFe_2Ge_2 [14, 17], (ii) modified flux growth (MF) from a polycrystalline YFe_2Ge_2 precursor with a reduced peak temperature between 850 and 1150 °C, or (iii) horizontal flux (or ‘liquid transport’ - LT) growth across a temperature gradient in a two-zone furnace with the cold end at 500 °C [19, 20]. The advantages of LT and MF growth vs. SF growth are discussed below. The in-plane electrical resistance was determined using a standard four-terminal *ac* technique in a Quantum Design Physical Properties Measurement System (PPMS) to < 0.4 K. Data were scaled at 300 K to the published high temperature resistivity of $190 \mu\Omega \text{ cm}$ [17]. Heat capacity measurements employed the pulse-relaxation method in a PPMS to below 0.4 K and a compensated heat pulse method in a $^3\text{He}/^4\text{He}$ dilution fridge to 50 mK [21]. The magnetization data were taken in a Cryogenic SQUID magnetometer to below 0.45 K and were corrected for the effect of demagnetizing fields by approximating the sample shape as a rectangular prism. Powder x-ray diffraction (XRD) patterns were collected at room temperature in the Bragg-Brentano geometry with $\text{Cu } K\alpha$ radiation at 40 kV and 40 mA on a Bruker D8 diffractometer equipped with a Lynxeye XE detector to reduce the effects of Fe fluorescence and $K\beta$ radiation. Refinements of the powder patterns showed no evidence of secondary phases except for occasional Sn flux inclusions. Lattice parameters were determined by referring to an internal Ge standard and using the Le Bail method.

Low-temperature heat capacity and electrical resistivity of YFe_2Ge_2 crystals from different growth batches are compared in Fig. 1. Crystals grown using standard flux methods (SF) have extrapolated $T = 0$ residual resistivity $\rho_0 \simeq 3.5 \mu\Omega \text{ cm}$, corresponding to $\text{RRR} \simeq 50 - 60$. Some of these samples show resistive transitions, but none display a superconducting heat capacity anomaly, confirming the findings of the previous single crystal study [14]. The modified flux growth from polycrystal precursors (MF) leads to a marked improvement, reaching $\rho_0 \simeq 1 \mu\Omega \text{ cm}$ and $\text{RRR} \simeq 200$ in the best batches. These samples show full resistive transitions, which often split into two steps, and they show broad heat capacity anomalies similar to those observed in the best polycrystals with similar RRR values [15, 16]. Crystals grown in

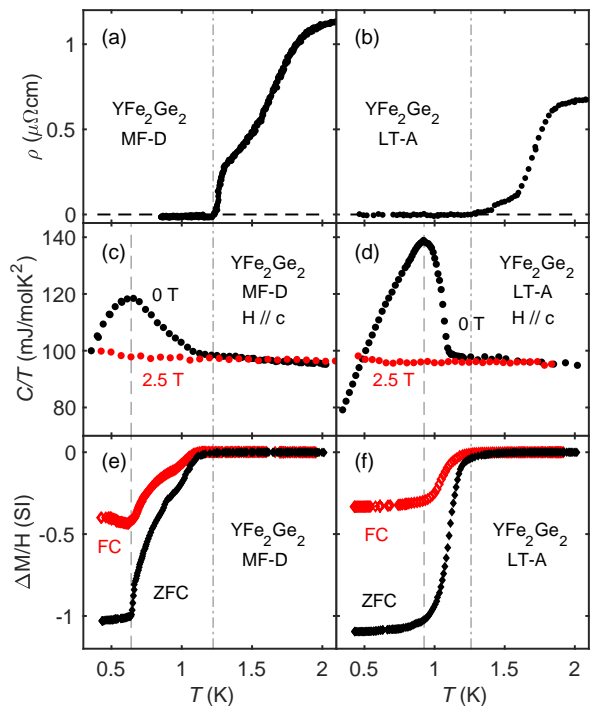


Figure 2. Electrical resistivity ρ [(a) and (b)], Sommerfeld coefficient of the heat capacity C/T [(c) and (d)] and magnetization (FC - field cooled, ZFC - zero-field cooled) [(e) and (f)] for two batches of high-quality YFe_2Ge_2 single crystals. The vertical dash-dotted lines denote the temperatures at which resistivity drops to zero in (a) and (b). The vertical dashed lines indicate the peaks of C/T in (c) and (d).

the liquid transport setup (LT) with a horizontal temperature gradient display the lowest residual resistivity $\rho_0 \simeq 0.45 \mu\Omega \text{ cm}$ and reach resistance ratios of up to $\text{RRR} \simeq 430$. These samples show sharp heat capacity jumps at a bulk T_c of about 1.1 K.

Resistive, thermodynamic and magnetic signatures of the superconducting transition in YFe_2Ge_2 in MF and LT samples are compared in Fig. 2. An applied magnetic field of 2.5 T completely suppresses superconductivity in both YFe_2Ge_2 samples (Figs. 2(c) and (d)), revealing the same underlying normal-state $C/T \approx 100 \text{ mJ/molK}^2$. SQUID magnetometry provides further evidence of bulk superconductivity in samples with $\text{RRR} \gtrsim 150$. The superconducting volume fraction inferred from the zero-field cooled diamagnetic response in Figs. 2(e) and 2(f) approaches 100% just below the peak of the specific heat transition for samples from batch MF-D and LT-A respectively. The complete diamagnetic screening in the magnetisation measurement and the sharp transition in heat capacity both suggest 100% bulk superconductivity in the high-quality samples. This is consistent with the mean free path ℓ and the scattering rate τ^{-1} extracted from resistivity measurements, using the approach described in [16]: the residual resistivity $\rho_0 \simeq 0.45 \mu\Omega \text{ cm}$ of LT-grown crystals translates to $\ell \simeq 2400 \text{ \AA}$, far larger

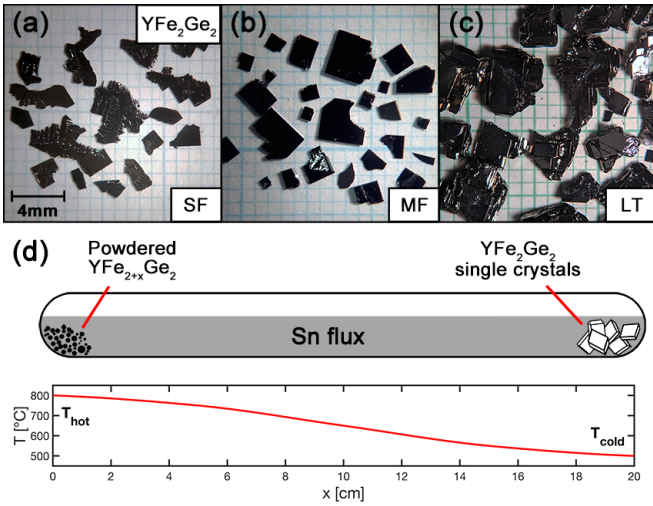


Figure 3. YFe₂Ge₂ single crystals produced using (a) SF, (b) MF and (c) LT methods on millimeter-scale paper. Dendrite formation is observed in the SF-grown crystals, which usually contain only one well defined facet along the [100] *a*-axis in each crystal. Crystals from the MF batches display less-obvious dendritic patterns, smoother surfaces and more rectangular shapes. Both the SF- and MF-grown crystals form thin plates, whereas those from the LT batch are bulkier in the [001] *c*-direction with thickness reaching up to 2 mm. (d) Schematic illustration of the liquid transport technique (LT).

than the coherence length $\xi \simeq 180 \text{ \AA}$ [15], and to $\tau^{-1} \simeq 0.09 \text{ meV}/\hbar$, well below the threshold of about 0.2 meV expected within the Abrikosov-Gorkov approach [16, 22] from the bulk T_c .

The three growth methods used in this study produce YFe₂Ge₂ crystals with different morphology, as illustrated in Fig. 3(a) to (c). Structural refinement of XRD data confirms an observation previously made in polycrystals [16], namely that improved crystal quality correlates with increasing *c*-axis lattice parameters (Fig. 4). This is consistent with Fe deficiency on the Fe site presenting the dominant source of disorder. This interpretation is further supported by single-crystal XRD at 100 K, which identifies significant Ge substitution on the Fe-site in the sample with the lowest RRR and *c*-axis lattice parameter (Batch SF-B) [19], whereas bulk superconducting samples showed no signs of Ge-Fe site disorder.

In standard flux growth, all elements are fully dissolved before crystals are formed on cooling. To achieve a high yield, this requires a low flux/charge ratio, which in turn leads to a high peak temperature, usually about $1200 \text{ }^\circ\text{C}$, and a high precipitation temperature. The schematic phase diagram in Fig. 5 illustrates the benefits of our alternative growth protocols. We attribute the difficulties in growing high quality YFe₂Ge₂ crystals by the SF method to (i) the formation of secondary phases such as YFe₆Ge₆ at $T > 1000 \text{ }^\circ\text{C}$, which affects the composition of the melt, and (ii) the position of the apex of

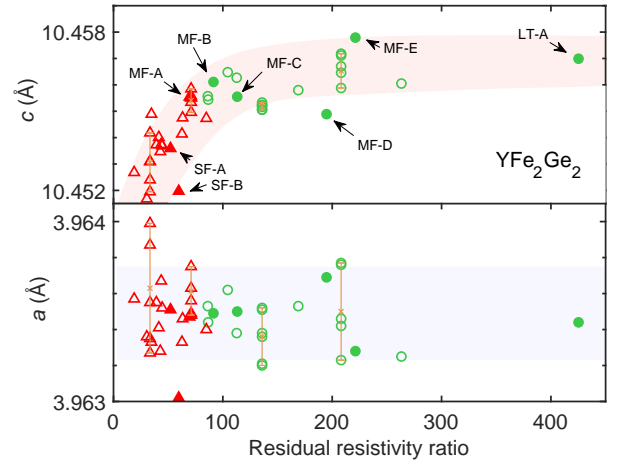


Figure 4. Lattice constants *c* (upper panel) and *a* (lower panel) of polycrystalline (open symbols) [16] and single-crystal (solid symbols) YFe₂Ge₂ samples, as obtained by powder XRD refinement, versus the corresponding RRR values. Green circles (red triangles) indicate that superconducting heat capacity anomalies have (have not) been observed. Errorbars are estimated from repeated measurements on selected batches of polycrystals. The pink and blue shades are guide to the eyes.

the narrow YFe₂Ge₂ homogeneity range at a slightly off-stoichiometric composition YFe_{2- δ} Ge_{2+ δ} , which favours Fe-poor crystals precipitating at high temperatures. In the modified flux method, the peak temperature can be reduced well below $\sim 1000 \text{ }^\circ\text{C}$, while maintaining stoichiometry in the melt thanks to the polycrystalline precursor. Because the precursor is not fully dissolved, the melt remains a saturated solution of YFe₂Ge₂ in Sn. The melt composition follows the liquidus curve from point A to point B as it heats up, gradually dissolving more of the charge. As the melt is cooled back down, it tracks the liquidus in reverse towards point C while precipitating YFe_{2- η} Ge_{2+ η} ($0 < \eta < \delta$). This process limits the crystal growth to the desired low temperature region of the liquidus in the complex quaternary phase diagram, avoiding the formation of secondary phases and facilitating the growth of crystals with higher Fe/Ge ratio, closer to the stoichiometric composition. The heating/cooling cycle $C \rightarrow B \rightarrow C$ can be repeated to increase yield: every heating segment preferentially dissolves small crystallites on the polycrystalline charge, whereas each cooling segment preferentially deposits onto larger crystals forming elsewhere in the crucible. YFe₂Ge₂ is thereby gradually transported from the polycrystal precursor towards the single crystals, keeping the desired stoichiometry intact. Using Fe-rich precursors may further encourage high Fe content in the crystals. However, because precipitation occurs over a range of temperatures, the resulting crystals exhibit some inhomogeneity of composition and disorder level, causing broad resistive and heat capacity anomalies.

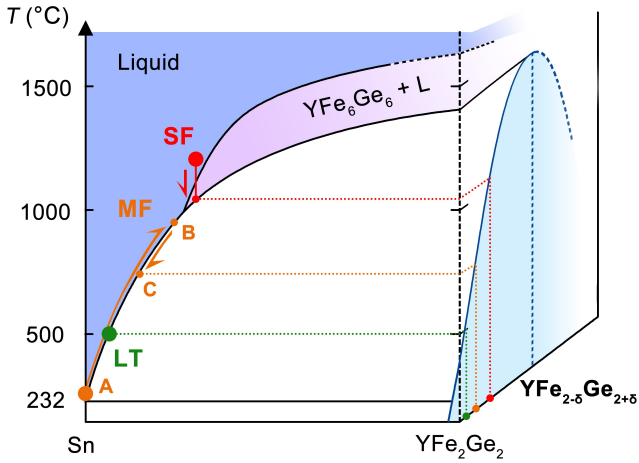


Figure 5. Schematic phase diagram illustrating YFe_2Ge_2 growth from Sn flux. SF growth proceeds from fully molten charge (red trajectory) and leads to Fe-poor crystals, if the apex of the $\text{YFe}_{2-x}\text{Ge}_{2+x}$ homogeneity range lies at an off-stoichiometric composition. MF growth proceeds from a saturated solution of YFe_2Ge_2 (orange trajectory), enabling a higher flux/charge ratio in the melt and consequently lower precipitation temperatures. It produces crystals with closer to the ideal stoichiometry, but with considerable inhomogeneity. LT growth precipitates at a well-defined, low temperature and produces the highest quality crystals. At temperatures above $\sim 1000^\circ\text{C}$ (purple zone), alien phases such as YFe_6Ge_6 may form, which affects the composition of the melt.

lies. Liquid transport growth extends the idea of using the flux to transport material from precursor towards crystals to a horizontal geometry. Maintaining a constant temperature at the cold end of the flux mixture ensures that crystal growth takes place at a fixed point on the liquidus. This improves homogeneity and reduces Fe-Ge site disorder, resulting in the sharpened bulk transition in crystals from Batch LT-A.

Low temperature heat capacity measurements (Fig. 6) in these samples show a specific heat jump $\Delta C(T_c)/T_c$ of only $\sim 40\%$ of the normal state Sommerfeld coefficient $\gamma_n \simeq 100 \text{ mJ/molK}^2$, significantly less than $\Delta C(T_c)/T_c \approx 1.43\gamma_n$ expected in a conventional s -wave superconductor but close to that observed in the isostructural compound KFe_2As_2 [4]. Extrapolating the linear temperature dependence of C/T observed below 0.7 K to $T = 0$ yields a residual Sommerfeld ratio $\gamma_0 \approx 0.4\gamma_n$ at zero field, which rises further as the applied field is increased (inset to Fig. 6).

Our findings mirror key results in iron arsenides such as $(\text{Ba/K})\text{Fe}_2\text{As}_2$. The fast suppression of bulk superconductivity by lattice disorder excludes a conventional isotropic s -wave scenario. The small $\Delta C(T_c)/\gamma_n T_c$ can be ascribed to multi-gap superconductivity, as in KFe_2As_2 [4, 23]. Likewise, the significant extrapolated residual Sommerfeld ratio γ_0 might point towards a further downturn in C_{el}/T at temperatures below the range

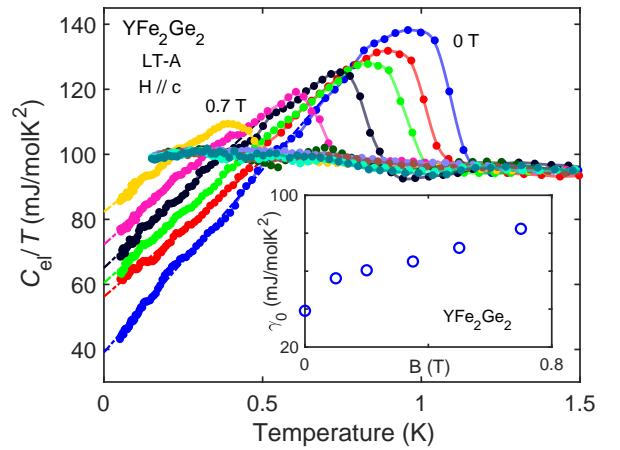


Figure 6. Electronic contribution to the specific heat capacity versus temperature, C_{el}/T , of a YFe_2Ge_2 single crystal from batch LT-A. Applied fields are 0 T (labelled), 0.1 T (red), 0.2 T (green), 0.35 T (black), 0.5 T (pink) (labelled) and 1 T (dark green). C_{el} is obtained by subtracting from the total specific heat capacity the fitted nuclear contribution $C_n(H, T) = \alpha(H)/T^2$ [19]. Inset: extrapolated zero-temperature residual C_{el}/T versus applied field.

of our current experiments, if the gap on part of the Fermi surface is much smaller than $k_B T_c$. However, because γ_0 rises with increasing disorder level, it is more plausibly attributed to impurity-induced states within the gap: The magnitude of γ_0/γ_n as well as its field dependence (Fig. 6) are similar to observations in some other iron-based superconductors (e.g. [24]). For sign-changing order parameters, e.g. a two-band s^\pm -wave model, a finite γ_0 at zero field and a linear temperature dependence of C/T at low T – as observed in YFe_2Ge_2 (Fig. 6) – are expected when the level of impurity scattering increases above a critical threshold [25]. The field dependence of γ_0 is also consistent with this scenario [26, 27], which is in line with earlier theoretical predictions [2] for YFe_2Ge_2 .

Liquid transport growth emerges as a powerful tool for growing large, high quality crystals of YFe_2Ge_2 and other challenging materials. It has enabled a seven-fold reduction in disorder level in the new generation of YFe_2Ge_2 crystals which, for the first time, show sharp thermodynamic transition anomalies indicative of bulk superconductivity. This will enable wide-ranging experiments probing superconducting and normal states in YFe_2Ge_2 . The disorder sensitivity of the superconducting transition in general and of the residual Sommerfeld coefficient in particular point towards a sign-changing order parameter.

We thank, in particular, A. Chubukov, C. Geibel, G. Lonzarich, J. Schmalian, F. Steglich and M. Sutherland for helpful discussions. The work was supported by the EPSRC of the UK (grants no. EP/K012894 and EP/P023290/1) and by Trinity College.

-
- * Now at Clarendon Laboratory, Department of Physics, University of Oxford, Oxford, OX1 3PU, United Kingdom
- [1] Y. Zou, Z. Feng, P. W. Logg, J. Chen, G. Lampronti, and F. M. Grosche, Fermi liquid breakdown and evidence for superconductivity in YFe_2Ge_2 , *Physica Status Solidi - Rapid Research Letters* **8**, 928 (2014).
 - [2] A. Subedi, Unconventional sign-changing superconductivity near quantum criticality in YFe_2Ge_2 , *Physical Review B - Condensed Matter and Materials Physics* **89**, 1 (2014).
 - [3] D. J. Singh, Superconductivity and magnetism in YFe_2Ge_2 , *Physical Review B - Condensed Matter and Materials Physics* **89**, 1 (2014).
 - [4] F. Hardy, R. Eder, M. Jackson, D. Aoki, C. Paulsen, T. Wolf, B. Anna, P. Schweiss, P. Adelman, R. A. Fisher, and C. Meingast, Multiband superconductivity in KFe_2As_2 : evidence for one isotropic and several Liliputian energy gaps, *J. Phys. Soc. Jpn.* **83**, 014711 (2014).
 - [5] A. F. Wang, B. Y. Pan, X. G. Luo, F. Chen, Y. J. Yan, J. J. Ying, G. J. Ye, P. Cheng, X. C. Hong, S. Y. Li, and X. H. Chen, Calorimetric study of single-crystal CsFe_2As_2 , *Physical Review B - Condensed Matter and Materials Physics* **87**, 2 (2013).
 - [6] S. Khim, S. Aswartham, V. Grinenko, D. Efremov, C. G. Blum, F. Steckel, D. Gruner, A. U. Wolter, S. L. Drechsler, C. Heß, S. Wurmehl, and B. Büchner, A calorimetric investigation of RbFe_2As_2 single crystals, *Physica Status Solidi (B) Basic Research* **254**, 1 (2017).
 - [7] Q. Si, R. Yu, and E. Abrahams, High-temperature superconductivity in iron pnictides and chalcogenides, *Nature Reviews Materials* **1** (2016).
 - [8] J. P. Reid, A. Juneau-Fecteau, R. T. Gordon, S. René De Cotret, N. Doiron-Leyraud, X. G. Luo, H. Shakeripour, J. Chang, M. A. Tanatar, H. Kim, R. Prozorov, T. Saito, H. Fukazawa, Y. Kohori, K. Kihou, C. H. Lee, A. Iyo, H. Eisaki, B. Shen, H. H. Wen, and L. Taillefer, From *d*-wave to *s*-wave pairing in the iron-pnictide superconductor $(\text{Ba},\text{K})\text{Fe}_2\text{As}_2$, *Superconductor Science and Technology* **25** (2012).
 - [9] F. Hardy, A. E. Böhmer, D. Aoki, P. Burger, T. Wolf, P. Schweiss, R. Heid, P. Adelman, Y. X. Yao, G. Kotliar, J. Schmalian, and C. Meingast, Evidence of strong correlations and coherence-incoherence crossover in the iron pnictide superconductor KFe_2As_2 , *Physical Review Letters* **111**, 1 (2013).
 - [10] Y. P. Wu, D. Zhao, A. F. Wang, N. Z. Wang, Z. J. Xiang, X. G. Luo, T. Wu, and X. H. Chen, Emergent Kondo Lattice Behavior in Iron-Based Superconductors AFe_2As_2 ($\text{A} = \text{K}, \text{Rb}, \text{Cs}$), *Physical Review Letters* **116**, 1 (2016).
 - [11] D. Zhao, H. L. Wo, J. Li, D. W. Song, L. X. Zheng, S. J. Li, L. P. Nie, X. G. Luo, J. Zhao, T. Wu, and X. H. Chen, Approaching itinerant magnetic quantum criticality through a Hund's coupling induced electronic crossover in the YFe_2Ge_2 superconductor, *Physical Review B* **101**, 1 (2020).
 - [12] A. Georges, L. de' Medici, and J. Mravlje, Strong Correlations from Hund's Coupling, *Annual Review of Condensed Matter Physics* **4**, 137 (2013).
 - [13] I. Felner, B. Lv, K. Zhao, and C. W. Chu, High-pressure resistivity of YFe_2Si_2 and magnetic studies of $\text{Y}_{1-y}\text{Ho}_y\text{Fe}_2\text{Si}_2$ and $\text{YFe}_2(\text{Si}_{1-x}\text{Ge}_x)_2$ systems, *Journal of Superconductivity and Novel Magnetism* **28**, 1207 (2015).
 - [14] H. Kim, S. Ran, E. Mun, H. Hodovanets, M. Tanatar, R. Prozorov, S. Bud'ko, and P. Canfield, Crystal growth and annealing study of fragile, non-bulk superconductivity in YFe_2Ge_2 , *Philosophical Magazine* **95**, 804 (2015).
 - [15] J. Chen, K. Semeniuk, Z. Feng, P. Reiss, P. Brown, Y. Zou, P. W. Logg, G. I. Lampronti, and F. M. Grosche, Unconventional superconductivity in the layered iron germanide YFe_2Ge_2 , *Physical Review Letters* **116**, 127001 (2016).
 - [16] J. Chen, M. B. Gamza, K. Semeniuk, and F. M. Grosche, Composition dependence of bulk superconductivity in YFe_2Ge_2 , *Physical Review B* **99**, 1 (2019).
 - [17] M. Avila, S. Bud'ko, and P. Canfield, Anisotropic magnetization, specific heat and resistivity of RFe_2Ge_2 single crystals, *Journal of Magnetism and Magnetic Materials* **270**, 51 (2004).
 - [18] P. C. Canfield and Z. Fisk, Growth of single crystals from metallic fluxes, *Philosophical Magazine B: Physics of Condensed Matter; Statistical Mechanics, Electronic, Optical and Magnetic Properties* **65**, 1117 (1992).
 - [19] See Supplemental Material at [URL], which includes Refs. [14, 16], for further details of crystal growth protocols, of single-crystal XRD refinement results, and of the analysis of nuclear contribution to specific heat in the LT-A sample. (2020).
 - [20] J.-Q. Yan, B. C. Sales, M. A. Susner, and M. A. McGuire, Flux growth in a horizontal configuration: An analog to vapor transport growth, *Physical Review Materials* **1**, 023402 (2017).
 - [21] H. Wilhelm, T. Lühmann, T. Rus, and F. Steglich, A compensated heat-pulse calorimeter for low temperatures, *Review of Scientific Instruments* **75**, 2700 (2004).
 - [22] A. A. Abrikosov and L. P. Gor'kov, Contribution to the theory of superconducting alloys with paramagnetic impurities, *Sov.Phys-JETP* **12**, 1243 (1961).
 - [23] K. Okazaki, Y. Ota, Y. Kotani, W. Malaeb, Y. Ishida, T. Shimojima, T. Kiss, S. Watanabe, C.-T. Chen, K. Kihou, C. H. Lee, A. Iyo, H. Eisaki, T. Saito, H. Fukazawa, Y. Kohori, K. Hashimoto, T. Shibauchi, Y. Matsuda, H. Ikeda, H. Miyahara, R. Arita, A. Chainani, and S. Shin, Octet-Line Node Structure of Superconducting Order Parameter in KFe_2As_2 , *Science* **337**, 1314 (2012).
 - [24] J. S. Kim, B. D. Faeth, Y. Wang, P. J. Hirschfeld, G. R. Stewart, K. Gofryk, F. Ronning, A. S. Sefat, K. Y. Choi, and K. H. Kim, Specific heat to H_{c2} : Evidence for nodes or deep minima in the superconducting gap of underdoped and overdoped $\text{Ba}(\text{Fe}_{1-x}\text{Co}_x)_2\text{As}_2$, *Physical Review B* **86**, 014513 (2012).
 - [25] Y. Bang and G. R. Stewart, Superconducting properties of the s^\pm -wave state: Fe-based superconductors, *Journal of Physics Condensed Matter* **29**, aa564b (2017).
 - [26] Y. Bang, Volovik Effect in the $\pm s$ -Wave State for the Iron-Based Superconductors, *Physical Review Letters* **104**, 217001 (2010).
 - [27] Y. Wang, J. S. Kim, G. R. Stewart, P. J. Hirschfeld, S. Graser, S. Kasahara, T. Terashima, Y. Matsuda, T. Shibauchi, and I. Vekhter, Volovik effect in a highly anisotropic multiband superconductor: Experiment and theory, *Physical Review B* **84**, 184524 (2011).